POLITECNICO
MILANO 1863

SCUOLA DI INGEGNERIA INDUSTRIALE
E DELL'INFORMAZIONE

EXECUTIVE SUMMARY OF THE THESIS

A semi-automatic pipeline for the assessment of cardiogenic emboli stroke risk using CFD simulations

TESI MAGISTRALE IN BIOMEDICAL ENGINEERING – INGEGNERIA BIOMEDICA

AUTHOR: Carlo Bettinelli

ADVISOR: Prof. Emiliano Votta

CO-ADVISOR: Francesco Sturla, Ione Ianniruberto

ACADEMIC YEAR: 2024-25

1. Introduction

Transcatheter Aortic Valve Implantation (TAVI), albeit revolutionary, is associated with several risks, including cerebrovascular events (CVE), e.g., cardiogenic embolic stroke. These events predominantly occur in the periprocedural period and are caused by the embolization of calcified debris or air bubbles that are transported by the blood stream from the Aortic Valve (AV) to the cerebral arteries, occluding them [1]. Although the causes are known, the factors influencing this potentially fatal event must be investigated to guarantee a proper prevention during the TAVI procedure.

The transport of debris particles by the bloodstream depends on aortic haemodynamic, which in turn depends on the Aortic Arch (AoArch) anatomy [2]. The latter may play a crucial role in determining the debris pathways.

On this basis, this study aims to investigating the impact of AoArch anatomy on AoArch fluid dynamics and on particle transport into the cerebral arteries, potentially revealing anatomical features that could be predictive of cardiogenic embolic stroke risk.

2. State of the art

Many studies have been aimed to assess the stroke risk, and some of these investigated also the role of aortic haemodynamic in embolic particle transport through the supra-aortic arteries to the cerebral circulation. However, the state-of-the-art study for the present work is represented by a previous MSc by Flaminia Stentella [3]. In that work, three anatomies, one per AoArch type, were reconstructed by patient-specific imaging to perform computational fluid dynamic (CFD) simulations with suitable Boundary Conditions (BCs), followed by Particle Tracking (PT) post-processing. That study had some limitations: a very small patient cohort, an approximate reconstruction of the supra-aortic vessels, and an unrealistic number of tracked particles. The present study further develops that previous work by introducing three main advancements: the refinement of the 3D geometrical models, the improved definition of inlet and outlet boundary

conditions (BCs), the more realistic definition of debris particles.

3. Materials and Methods

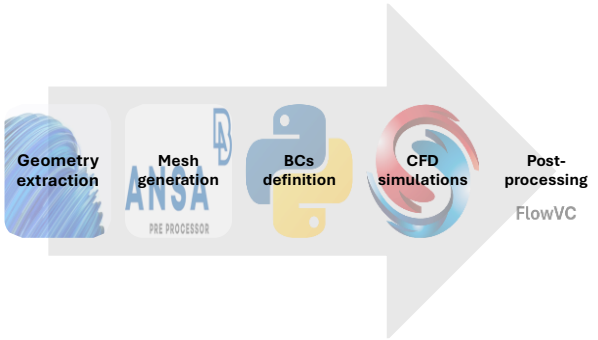

Figure 1: workflow macro-phases and mainly used tools.

The study workflow was characterized by five main stages (Figure 1), explained in the following subsections.

3.1. Image segmentation and mesh generation

Using the dynamic region growing method available in Materialise Mimics, patient-specific anatomical models were obtained by segmenting Computed Tomography (CT) scans and Phase-Contrast Magnetic Resonance Angiography (PC-MRA) of three patients characterized by type I, type II and type III arch type, respectively. The three models were named 1A, 2A, and 3A, respectively, and were added to those from [3], which were characterized by type I arch (1B model) and type III arch (3B anatomy), respectively. Model 1B was corrected through the segmentation of 4DFlow Visualization Toolkit (VTK) data to obtain an inlet section orthogonal to the local aorta axis (Figure 2).

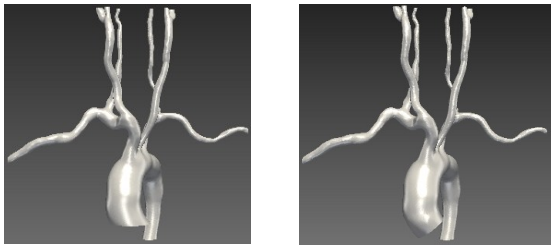

(A) (B)

Figure 2: model 1B before correction (A, [3]) and after correction (B) of the inlet region.

Each model included ascending aorta (AAo), AoArch, descending aorta (DAo), and main supra-aortic branches. The 3D geometrical models were discretized into tetrahedral elements through ANSA (BETA-CAE). Element dimension was automatically reduced at the supra-aortic vessels (Figure 3). The final element size resulted from a Mesh Sensitivity Analysis (MSA).

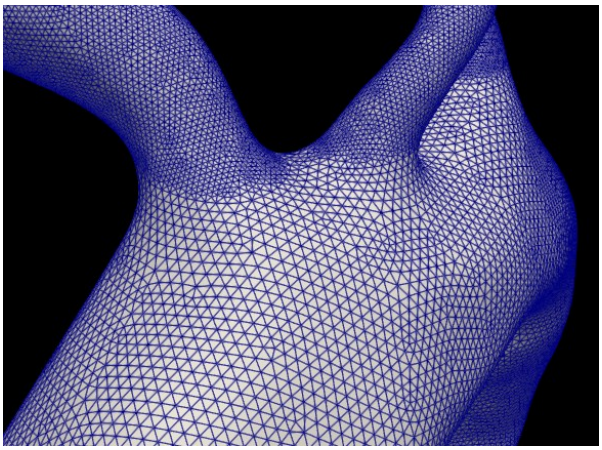

Figure 3: example of mesh obtained by ANSA, with local mesh refinement at the supra-aortic.

3.2. Boundary Conditions definition

Similarly to [3], the aortic wall was modelled as rigid and with no displacement. BCs were instead defined through a new two-step approach based on the coupling between the 3D domain and a 3-element Windkessel (WK) model at each outlet.

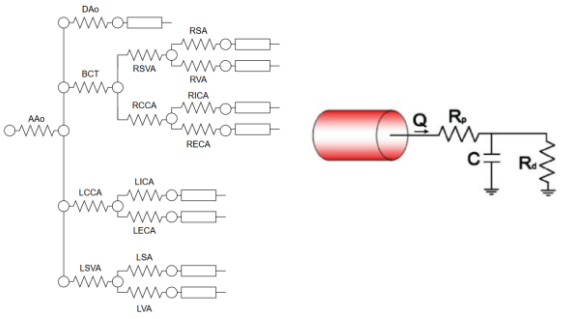

(A) (B)

Figure 4: (A) LPM general representation of the 3D models; (B) 3-Element Windkessel Model at each outlet. To initially calibrate R_p and R_d, the compliance C was neglected.

First, the resistances of the WK model were initialized based on the method proposed by Pirola [4] and automatically tuned through stationary

simulations performed on anatomy-dependent Lumped-Parameter Models (LPM), which accounted for aortic centerline features and 3D anatomical features (Figure 4A). LPM-based simulations were run through the Zero-Dimensional Solver (svZeroDSolver) available in SimVascular and yielded the set of WK resistances that allowed to reproduce the inlet and the outlets pressures. Second, the final tuning of the parameters of WK resistances was performed (i) to align the inlet pressure level to the Mean Arterial Pressure (MAP) (~ 93mmHg) and (ii) to ensure the physiological flow split, defined with literature study on vessels flow rate (e.g., [5], [6], [7]) or commonly used assumptions (e.g., [8]). Final RCR parameters (compliance C, proximal and distal resistances R_p and R_d, Figure 4B) were computed with literature formulas (e.g., [4], [9]).
The influence of inlet BCs was quantified: for each model, the patient-specific time-dependent flow rate at the aortic inlet was measured from 4DFlow imaging. The same flow rate condition was imposed through two different inlet velocity profiles: i) 4DFlow-derived and ii) plug.

3.3. CFD simulations

For each patient-specific model and for both inlet velocity profiles, CFD transient simulations were run through the solver SimVascular FSI (svFSI). Navier-Stokes equation (1) was solved with its stabilized weak form, assuming blood as a Newtonian incompressible fluid ($\rho = 0.00106\text{g/mm}^3$, $\mu = 0.004\text{Pa} \cdot \text{s}$) [10].

$$\rho\left(\frac{d\boldsymbol{u}}{dt} + \boldsymbol{u} \cdot \nabla \boldsymbol{u}\right) = -\nabla p + \mu \nabla^2 \boldsymbol{u} + b \qquad (1)$$

Courant-Friedrichs Lewy (CFL) condition was computed for each anatomy, confirming an acceptable accuracy ($\text{CFL} < 1$) given by the low timestep (1ms) balancing the lowest dimension element (0.125mm). CFD models are qualitatively and quantitatively validated by comparing the results with 4DFlow data.

3.4. Particle Tracking

CFD simulations post-processing was performed through FlowVC, a Lagrangian Particle Tracer (LPT) software. Spherical particles were seeded from a cube in the AAo (Figure 5), and were assigned different densities (0.8g/cm^3, 1.06g/cm^3, 1.22g/cm^3, 1.45g/cm^3), as in [3], and dimensions (325µm, 750µm, 1250µm) and numerosity (125 small particles, 27 medium particles, 8 large particles) based on literature data [11].

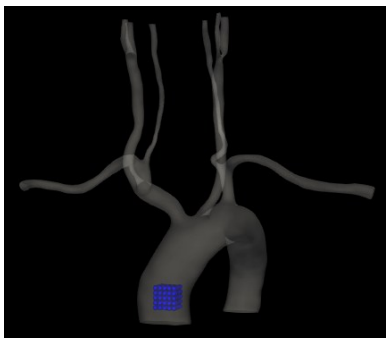

Figure 5: Region defined to seed debris particles in the AAo (blue).

4. Results

Mesh Sensitivity Analysis: Roache's Grid Convergence Index (GCI) computation has demonstrated the asymptotical convergence of the mesh ($k = 0.96 \sim 1$) with a higher GCI for maximum velocity in the AAo ($\text{GCI} = 0.14 - 0.25$) than GCIs for mean and maximum velocities of the finer mesh regions, e.g., the left subclavian artery ($\text{GCI}_{\text{mean,vel}} = 0.016 - 0.061$). Mean and maximum pressure showed approximatively null GCI and reached the asymptotic convergence ($k \sim 1$).
Model validation: CFD models were validated by comparing computed mean velocities vs. 4DFlow velocity data at peak systole at four cross-sectional planes (AAo, AoArch, isthmus, DAo), and by comparing computed flow rates vs. literature reference values.
Computed percentage flow rates in the supra-aortic vessels differed from literature-derived reference values (e.g., [5], [6], [7], [8]) by less than 1%; larger mismatches (2-5%) were observed in the descending aorta (Dao) and are likely due to the inability of the aortic LPM to exhaustively reproduce the features of the 3D geometry. Comparison between CFD mean velocity time-courses showed an excellent correlation with 4DFlow-derived ground truth ($r \sim 1$). Mean Absolute Error (MAE) vs. 4DFlow data was lower for the AAo slice ($<50\text{mm/s} = 5\text{cm/s}$), as expected because of the inlet BCs. MAE was greatest at the isthmus ($70 - 125\text{mm/s} = 7 - 12\text{cm/s}$), probably because of the haemodynamic disturbance in that region, and intermediate at the DAo ($38 - 90\text{mm/s} = 3.8 - 9\text{cm/s}$), possibly because of small errors

in flow split. Root Mean Squared Error (RMSE) values for every patient were slightly higher than MAE, as RMSE is by construction more influenced by high errors; however, RMSE data confirmed the discrepancies quantified by MAE. Velocity field comparison between CFD simulations and 4DFlow data showed consistency in terms of high-velocity regions, despite differences by about $10-30$cm/s for the most distal Dao slice, where inaccuracies in flow split influenced the results. Velocity vectors comparison showed similar vectors orientation, confirming that CFD results captured the in vivo velocity directionality, in particular at the DAo slice (Figure 6D), where blood flow is more developed. Flow directionality was captured with lowest accuracy at the AAo, because of a not fully developed flow, and at the isthmus slices (Figure 6A, Figure 6C). Across all the patients, the use of a plug inlet profile and a patient-specific profile led to similar time-course of flow rate and pressure: differences were confined to the AAo slice, suggesting that an idealized inlet BC may be acceptable when patient-specific profiles are not available.

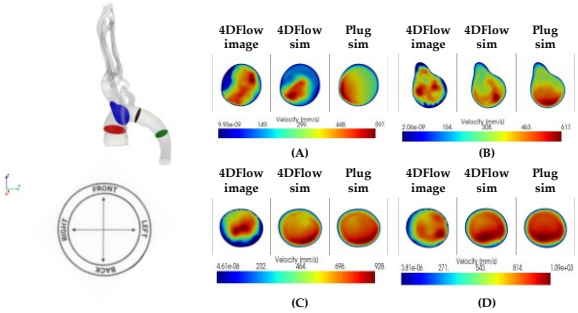

Figure 6: validation of CFD results with respect to the 4DFlow velocity data for patient 1B. (A: red slice, middle AAo, B: blue, middle AoArch, C: black, isthmus, D: green, middle DAo).

***Particle tracking analyses*:** Comparison of particle end positions for each anatomy (Table 2) showed that type II arch is more prone to cardiogenic embolic stroke risk: it is characterized by the lowest particles percentage remaining in the AoArch (<85%), and particles are mainly transported in the brachiocephalic trunk. Conversely, type III is the least prone to stroke risk, because of its highest percentages of particles remaining in the AoArch (>95%) and the few particles transported through supra-aortic branches mainly end their path in the left subclavian artery. This outcome was observed already in [3], suggesting that AoArch type may influence the cardiogenic embolic stroke risk.

Table 1: density comparison for small particles (dimension: 325µm, total number: 125) in patient 3B (type III) for both the inlet profiles.

Density [g/cm^3]	Profile	% AoArch	% BCT	% LCCA	% LSVA
0.8	**4DFlow**	95.2	0	0	4.8
	Plug	98.4	0	0	1.6
1.06	**4DFlow**	96.8	0	0	3.2
	Plug	99.2	0	0	0.8
1.22	**4DFlow**	96	0	0	4
	Plug	99.2	0	0	0.8
1.45	**4DFlow**	96.8	0	0	3.2
	Plug	99.2	0	0	0.8

Density comparison (Table 1) suggests that heavier particles are more prone to remain in the AoArch, while lighter particles are more prone to enter the supra-aortic branches. However, this trend was less clear when 4DFlow-derived velocity profiles were imposed at the inlet, possibly because of the associated more complex fluid dynamic patterns in the Aao.

Table 2: percentage of particles entering the branches of the model for each model and inlet velocity profile. Data refer to small thrombotic particles (density: 1.06g/cm^3, dimension: 325µm, total number: 125)

Patient	Profile	% AoArch	% BCT	% LCCA	% LSVA
1A	**4D**	84.8	8	0	7.2
	Plug	93.6	0	0	6.4
1B	**4D**	86.4	3.2	4	6.4
	Plug	89.6	0.8	3.2	6.4
2A	**4D**	84	12	2.4	1.6
	Plug	82.4	7.2	0	9.6
3A	**4D**	94.4	0.8	0	4.8
	Plug	98.4	0	0	1.6
3B	**4D**	96.8	0	0	3.2
	Plug	99.2	0	0	0.8

The models characterized by Type I AoArch did not share similar percentages of particles transported in the different branches, suggesting that other anatomical features, e.g., the shape of the AAo or the tortuosity of the supra-aortic branches, can influence the embolic pathways.

The percentage of particles entering the different branches was influenced by the inlet velocity profile (4DFlow-based vs. plug): although the three supra-aortic branches altogether received the same percentage of particles, the repartition among them changed, especially for models with type I and II AoArch (Table 1). However, in every model and for every inlet velocity profile a non-zero percentage of particles entered the left subclavian artery (LSVA), suggesting that a cerebroembolic protection is potentially always required for this artery (Table 2).

5. Limitations and future developments

Despite the innovations introduced with respect to [3], this study is not exempt from limitations:

- **Computational time**: CFD simulations are known to be time expensive. Mesh optimization improved this aspect, but the overall model is not yet intended to be suitable for TAVI-planning. It is suggested to investigate the potential of ANSA to further optimize mesh generation.
- **Patient-specificity of flow split**: despite the good reproduction of target flow split, the proposed LPM-based calibration of outlet BCs appears to be insufficient to represent patient-specific haemodynamic, as observed by errors at DAo sections. The potential of svZeroDSolver must be investigated to provide a more accurate or also time-dependent calibration.
- **PT plausibility**: the reduction of the particle number as compared to [3] allowed to consider more realistic conditions. However, the assumed number of seeded particles is based on the amount of particles captured by filters in previous clinical studies, which may be an underestimation of the amount of particles detaching from the Aao, which could be estimated even more realistically. Furthermore, particles may be modelled not only as spheres, because in the real word particles are not perfectly spherical-shaped.
- **Segmentation method and patient cohort**: dynamic region growing is not a fully automatic method and multiple manual interventions are required to obtain the final 3D reconstruction. Furthermore, the cohort of five patients, despite representing all the AoArch types, was not sufficient to define robust anatomical criteria leading to a major cardiogenic embolic stroke risk. The extension of the cohort, possibly including also odd branching patterns such as the bovine AoArch, is a fundamental future direction. The development of a fully automated and reliable segmentation method would facilitate the analysis of large cohorts.

The long-term goal of the study is to provide a computational tool to assist TAVI planning, potentially based on the visualization of patient-specific imaging to assess the CVE risk from its AoArch and supra-aortic arteries anatomical details. Albeit necessary in this early phase to collect preliminary data and information, CFD simulation may be no longer utilized.

6. Conclusions

Despite the reported limitations, it is possible to conclude that cardiogenic embolic stroke risk may be influenced by many factors, e.g., particle density or the AoArch anatomical features: AoArch type and the patient-specific anatomical details characterizing the supra-aortic arteries and the aorta are aspects to consider for the adoption of personalized TAVI-planning approach. CFD simulations and PT post-processing may be used to predict probable particle paths based on pre-procedural imaging.

References

[1] A. Postolache et al., "TAVI after More Than 20 Years," *Journal of Clinical Medicine*, vol. 12, no. 17, p. 5645, 30 August 2023.

[2] M. M. Marrocco-Trischitta et al., "Blood flow helical pattern in type III arch configuration as a potential risk factor for type B aortic dissection," *European Journal of Cardio-Thoracic Surgery*, vol. 61, no. 1, pp. 132-139, 10 August 2021.

[3] F. Stentella, ""Image-based computational fluid dynamics to assess the effect of aortic arch morphology on cardiogenic embolic

transport to the brain",” 2024. [Online]. Available: https://hdl.handle.net/10589/231365.

[4] S. Pirola et al., “On the choice of outlet boundary conditions for patient-specific analysis of aortic flow using computational fluid dynamics,” *Journal of Biomechanics,* vol. 60, pp. 15-21, 1 August 2017.

[5] P. Reymond et al., “Validation of a one-dimensional model of the systemic arterial tree,” *American Journal of Physiology - Heart and Circulatory Physiology,* vol. 297, no. 1, pp. H208-H222, 2009.

[6] S. O. Oktar et al., “Blood-Flow Volume Quantification in Internal Carotid and Vertebral Arteries: Comparison of 3 Different Ultrasound Techniques with Phase-Contrast MR Imaging,” *American Journal of Neuroradiology,* vol. 27, no. 2, pp. 363-369, February 2006.

[7] B. Hennen et al., “Do Changes in Blood Flow in the Subclavian Artery Affect Flow Volume in IMA Grafts After Complete Arterial Revascularization with the T-Graft Technique?,” *The Thoracic and Cardiovascular Surgeon,* vol. 49, no. 2, pp. 84-88, 2001.

[8] A. Ruggeri et al., “Patient-specific computational fluid hemodynamics in the ascending aorta before and after thoracic endovascular repair,” *Computers in Biology and Medicine,* vol. 194, p. 110493, 3 June 2025.

[9] R. Tricarico et al., “Non-invasive estimation of the parameters of a three-element windkessel model of aortic arch arteries in patients undergoing thoracic endovascular aortic repair,” *Front Bioeng Biotechnol.,* no. 11:1127855, (2023).

[10] “svMultiphysics,” Stanford University, [Online]. Available: https://simvascular.github.io/documentation/multi_physics.html#numerical_linear_algebra.

[11] T. Schmidt et al., “Debris Heterogeneity Across Different Valve Types Captured by a Cerebral Protection System During Transcatheter Aortic Valve Replacement,” *JACC,* vol. 11, no. 13, pp. 1262-1273, 2018.